Processing conditions and microstructural features of porous 316L stainless steel components by DMLS

Dongdong Gu *, Yifu Shen

College of Materials Science and Technology, Nanjing University of Aeronautics and Astronautics, 29 Yudao Street, 210016 Nanjing, PR China

A R T I C L E   I N F O

A B S T R A C T

Direct metal laser sintering (DMLS), due to its flexibility in materials and shapes, would be especially interesting to produce complex shaped porous metallic components. In the present work, processing conditions and microstructural characteristics of direct laser sintered porous 316L stainless steel components were studied. It was found that a partial melting mechanism of powders gave a high feasibility in obtaining porous sintered structures possessing porosities of $\sim$21–$\sim$55%. Linear energy density (LED), which was defined by the ratio of laser power to scan speed, was used to tailor the laser sintering mechanism. A moderate LED of $\sim$3400–$\sim$6000 J/m and a lower scan speed less than 0.06 m/s proved to be feasible. With the favorable sintering mechanism prevailed, lowering laser power or increasing scan speed, scan line spacing, and powder layer thickness generally led to a higher porosity. Metallurgical mechanisms of pore formation during DMLS were addressed. It showed that the presence of pores was through: (i) the formation of liquid bridges between partially melted particles during laser irradiation; and (ii) the growth of sintering necks during solidification, leaving residual pores between solidified metallic agglomerates.

1. Introduction

Porous metals are known to have many interesting combinations of physical and mechanical properties such as low specific weight, high gas permeability, and high thermal conductivity [1,2]. Therefore, there exists a growing interest in their practical applications in various industrial sectors such as automotive industry, aerospace industry, sporting equipment, and biomedical industry [3]. So far, a number of approaches concerning the fabrication of porous metals have been reported, including sintering of metal powders [4,5], foaming of slurries [6,7], and casting methods [8,9]. However, a common limitation of the powder sintering method is that pore characteristics (e.g., size, shape, and distribution of pores) are usually difficult to control [10]. Foaming approaches also have inherent limitations, such as contamination, formation of impurity phases, and limited control over pore features [11]. More important, porous metallic components with complex geometric features usually cannot be easily fabricated using the above mentioned conventional methods [12,13]. Thus, novel fabrication methods for porous metals should be innovatively designed to ensure complex part geometries coupled with controllable pore size, shape, and distribution.

Direct metal laser sintering (DMLS), as a typical solid freeform fabrication (SFF) technique, enables the quick production of complex shaped three-dimensional (3D) parts directly from metal powder [14–18]. The DMLS process creates parts in a layer-by-layer fashion by selectively fusing and consolidating thin layers of loose powder with a scanning laser beam. DMLS, due to its flexibility in materials and shapes, would be especially interesting to produce complex shaped porous metallic components. However, most of the previous work using DMLS has been focused on net shape manufacturing of fully dense metallic prototypes and tools [19–22]. Actually, few research efforts have been devoted in understanding how the porous structures are developed in DMLS-processed porous metals.

In this work, DMLS of 316L stainless steel (SS) powder was performed for the preparation of porous components. The processing conditions, microstructural features, and mechanical properties of DMLS-processed porous metals were assessed and the formation mechanisms of pores were elucidated. These principles are generic and can be applied to other pre-alloyed metallic materials with incongruent melting temperatures.

* Corresponding author. Tel.: +86 25 52112904 80517; fax: +86 25 52112626.
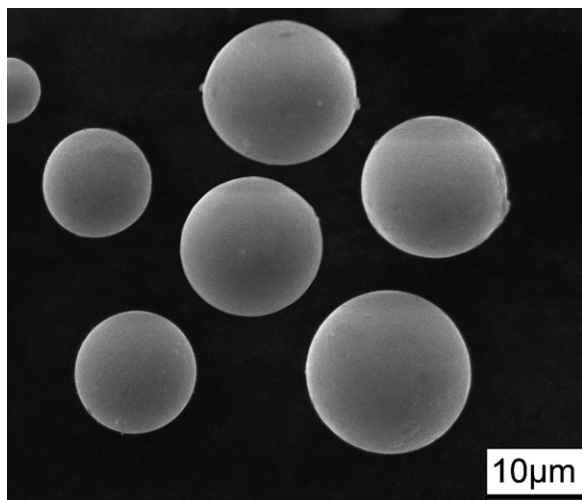 E-mail addresses: dongdonggu@nuaa.edu.cn, dongdonggu@hotmail.com
(D. Gu).

Fig. 1. SEM image showing characteristic morphology of SS powder.

2. Experimental

The austenitic 316L SS powder (supplier: Haining Feida Metallurgy Powder Co., Ltd. China) with a spherical shape and a mean particle size of 20 μm was used in the present study, as shown in Fig. 1. The elemental compositions of SS powder were: 16.9Cr, 13.2Ni, 2.7Mo, 1.6Mn, 0.019C, 0.23Si, Fe balance.

The used DMLS system, as schematically shown in Fig. 2a, consisted mainly of a continuous wave Gaussian CO_2 laser (type: Rofin-Sinar 2000SM, supplier: Rofin-Sinar Laser GmbH) with a maximum output power of 2000 W, an automatic powder delivery system, and a computer system for process control. Single layer sintering tests were primarily performed by repeated scanning a powder layer (0.15 mm in thickness) in order to establish a process map. Each single layer sintering test was processed within a 20 mm × 10 mm region. A simple linear raster scan pattern was used, as illustrated in Fig. 2b. From these preliminary experiments, a series of processing parameters were chosen for further preparation of multi-layer samples. When a sample was to be prepared, a steel substrate was placed on the building platform and leveled. Afterwards, a thin layer of loose SS powder was spread on the substrate by the roller. Subsequently, a laser beam scanned powder bed surface to form a layerwise profile according to CAD data of the sample. The similar process was repeated and the sample was produced layer by layer until completion. The used processing conditions were: spot size (D) 300 μm, laser power (P) 100–550 W, scan speed (v) 0.03–0.10 m/s, scan line spacing (h) 0.10–0.30 mm, and powder layer thickness (d) 0.10–0.25 mm.

The porosity of laser sintered porous samples was calculated using the following expression:

$$\text{Porosity} = 1 - \frac{\text{Mass of the porous metal}}{\text{Volume of the porous metal} \times \text{Density of the solid metal}} \qquad (1)$$

Surface morphologies of laser sintered samples were characterized using a Quanta 200 scanning electron microscope (SEM), operated at an accelerating voltage of 20 kV. The laser sintered porous samples were cut using a spark-erosion wire cutting machine to prepare standard specimens for tensile tests. The tensile directions were parallel to the sintered layers and parallel to the building direction (i.e., perpendicular to the sintered layers), respectively. Uniaxial tensile tests were performed at room temperature with a universal testing machine (type: CMT5105, supplier: Shenzhen

SANS Testing Machine Co., Ltd. China) at a strain rate of 10^{-3} s^{-1}. The ultimate tensile strength was determined from the stress–strain curve.

3. Results and discussion

3.1. Process map for porous structure

In order to determine a suitable process window within which laser sintering of SS powder would yield a desired porous structure, a series of laser power and scan speed combinations, as indicated by four sets of symbols in Fig. 3, were used to scan over the powder bed. Laser processing using the processing parameters denoted by the same symbols produced a similar sintering mechanism. With these key parameters points fixed, the boundary locations between the four different zones were determined. The powder melting mechanisms corresponding to the four process windows were defined as follows:

 (I) No melting: the delivered laser energy was insufficient to exert any effect on the powder, leaving a large amount of remaining unsintered starting powder particles.
 (II) Partial melting: at a moderate laser power combined with a low scan speed (<0.06 m/s), the liquid phase presented by means of the surface melting of particles, thus joining the unmelted cores of particles via liquid "bridge" to form a porous surface.
(III) Melting with balling: at a high laser power and a high scan speed (≥0.06 m/s), long, thin, and cylindrical shaped liquid
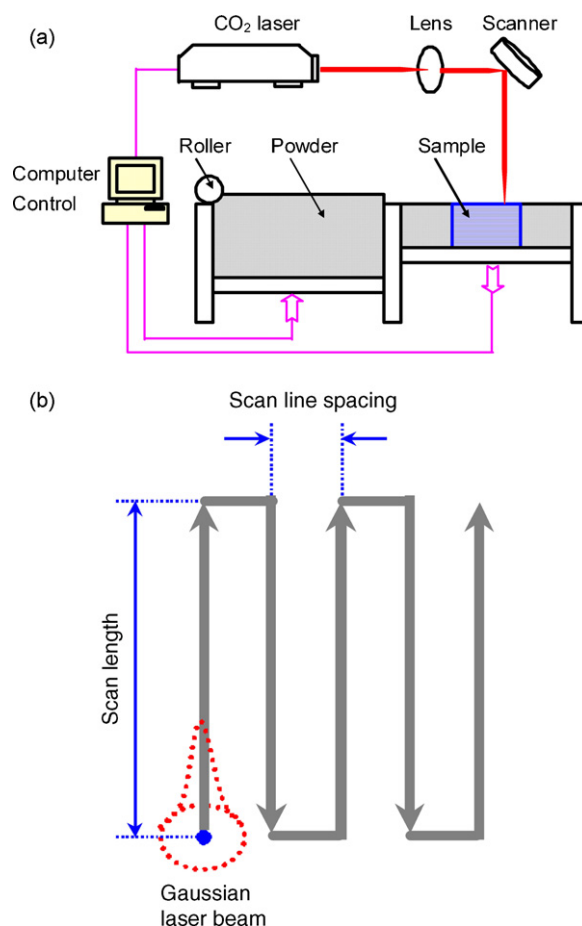

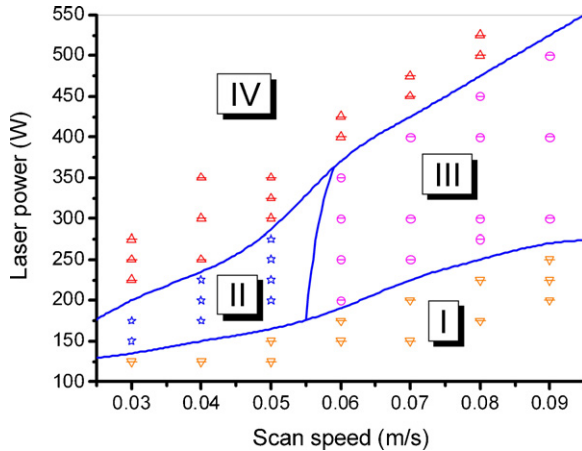**Fig. 2.** Schematics of laser sintering apparatus (a) and laser scanning pattern (b).

Fig. 3. Process map for laser sintering of a single layer of SS powder using a wide range of laser powers and scan speeds. Sintering mechanisms and resultant sintered structures are: Zone I—no melting, powder unsintered; Zone II—partial melting, porous sintered surface; Zone III—melting with balling, coarsened metallic balls; Zone IV—complete melting, fully dense sintered surface.

scan tracks were generated, which subsequently broke up into rows of coarsened metallic balls as a result of surface tension reduction.

(IV) Complete melting: the incident laser energy was great enough to produce continuous tracks of molten liquid, forming coherent sintered lines and a fully dense surface after solidification.

Typical processing parameters within different windows in Fig. 3 were chosen to prepare multi-layer components, with characteristic surface morphologies provided in Fig. 4. Laser sintering at a laser power of 300 W and a scan speed of 0.05 m/s (Zone IV) yielded continuous scan tracks and coherent inter-track bonding, showing a fully dense sintered surface (Fig. 4a). However, at a higher scan speed of 0.08 m/s, laser sintering at the same laser power (Zone III) produced discontinuous scan tracks consisting of significantly coarsened individual agglomerates in a spherical shape (Fig. 4b). Thus, it was confirmed that "balling" effect initiated in this instance. With the occurrence of balling, no effective inter-ball and inter-track bonding was obtained (Fig. 4b). Interesting, the sample processed at a lower laser power of 250 W and a scan speed of 0.05 m/s (Zone II) showed a desirable porous structure, which was characterized by open pores formed in sample surface. Moreover, the sintered surface consisted of continuous long bar-shaped metallic agglomerates, rather than
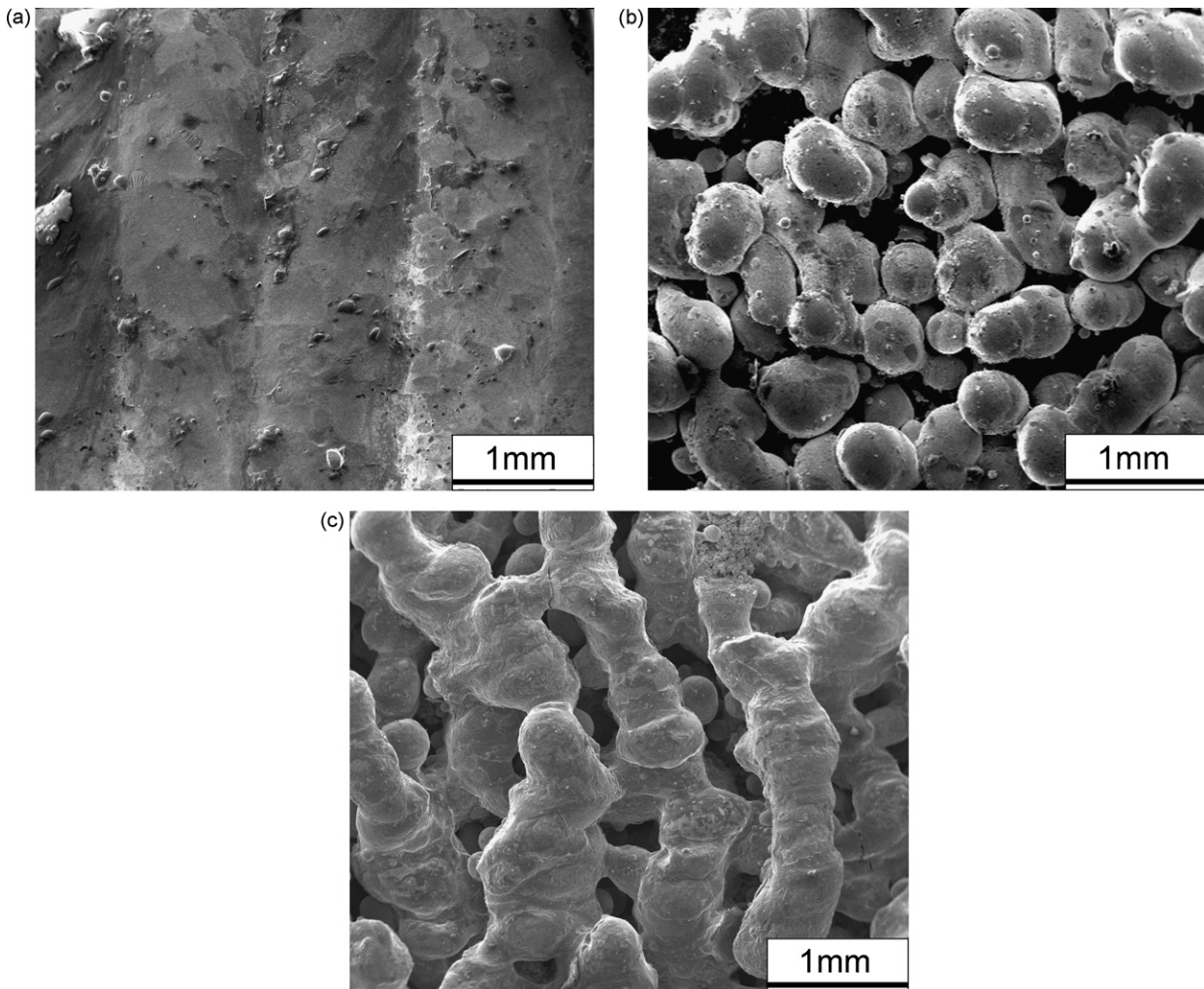

Fig. 4. SEM images showing surface morphologies of laser sintered samples prepared with typical parameters within different zones in Fig. 3: (a) P = 300 W, v = 0.05 m/s; (b) P = 300 W, v = 0.08 m/s; (c) P = 250 W, v = 0.05 m/s. Fixed parameters are h = 0.15 mm and d = 0.15 mm.
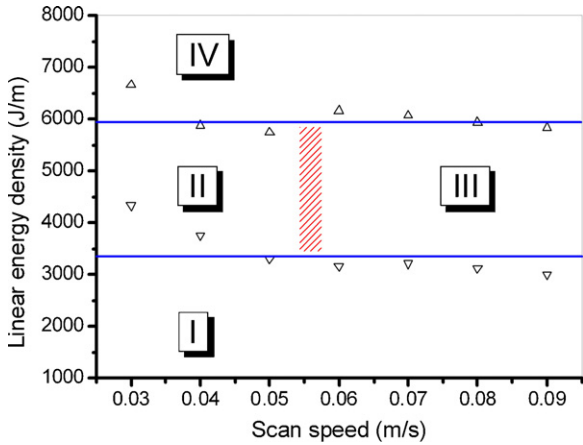
Fig. 5. Change of laser sintering mechanisms of SS powder with linear energy density. Note: boundary location between Zone II and Zone III is not absolutely strict due to the span of parameters choice (i.e., 0.01 m/s).

ball-like agglomerates (Fig. 4c). Therefore, the inherent weakness/brittleness incurred by balling effect could be well eliminated.

The establishment of the four process windows gave a high facility in choosing the suitable processing conditions under which laser sintering could generate a desired porous sintered structure. A close look at the parameter-dependent process map (Fig. 3) and the corresponding microstructural features (Fig. 4) revealed that the process window for the formation of porous structure was quite narrow. Processing parameter, especially laser power and

scan speed, were required to be carefully tailored in order to realize a feasible sintering mechanism by means of the partial melting of the powder.

In the case of pre-alloyed SS powder, melting occurs over a temperature range between the solidus and liquidus temperatures. The amount of liquid formation depends on the sintering temperature, which is in turn related to the energy gain of the powder [23]. It is known that an individual line scan introduces two main parameters, i.e., laser power and scan speed. In order to evaluate their combined influence, a new parameter, i.e., linear energy density (LED), is defined by the ratio of the incident laser power to the laser scan speed. After converting Fig. 3 into Fig. 5 using the defined LED, the relationship between the sintering mechanisms and the incident LED is clearly revealed. The LED should be strictly tailored, in order to obtain a suitable amount of liquid formation. The complete melting of SS powder is expected to occur at a LED larger than ~6000 J/m (Zone IV, Fig. 5), favoring the formation of fully dense sintered layers (Figs. 3 and 4a). Setting a lower LED between ~3400 and ~6000 J/m (Zone II, Fig. 5) is required for obtaining a desired porous structure (Figs. 3 and 4c). A decrease in LED (i.e., P/v) can be realized by increasing scan speed or decreasing laser power. However, using a higher scan speed, to a great extend, would result in the occurrence of balling (Figs. 3 and 4b), although the obtained LED can also falls within this favorable range (Zone III, Fig. 5). In this instance, laser sintering at a relatively higher LED above ~3400 J/m causes the melting along a row of powder particles, forming a continuous liquid scan track in a cylindrical shape. However, a higher scan speed (≥0.06 m/s) induces a significant capillary instability effect of the melts [24]. The diminishing in the surface energy of the molten track is going
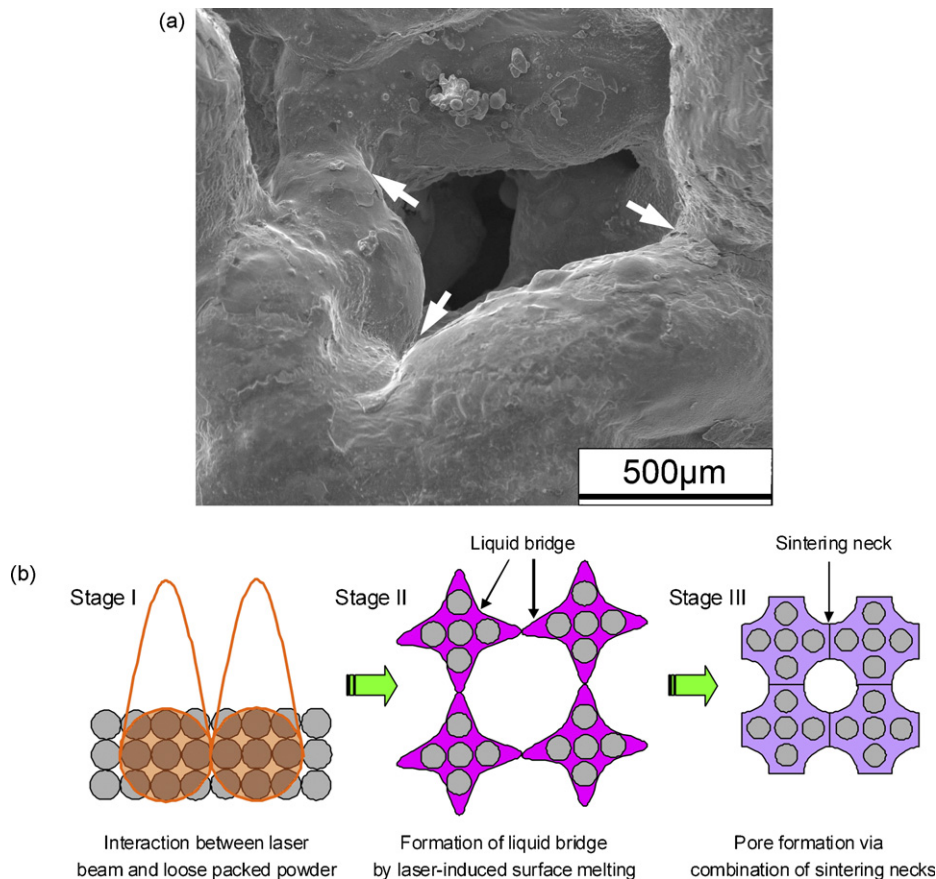

Fig. 6. High-magnified SEM image of Fig. 4c showing pore characteristics (a); schematic of pore development during DMLS (b).

on until the final equilibrium state through breaking up the cylinder into several metallic agglomerates in a spherical shape is obtained (so-called "balling" effect). Balling phenomenon, although it can also produce a certain amount of porosity in laser sintered layer, is a severe impediment to the smooth spreading of the fresh powder on the previously sintered layer and tends to cause delamination induced by poor inter-layer bonding in combination with thermal stresses, handicapping the completion of a multi-layer component. In the present study, a close study of Figs. 3–5 reveals that setting a moderate LED of ∼3400–∼6000 J/m and a lower scan speed less than 0.06 m/s proves to be an efficient method for obtaining a porous component free of balling.

3.2. Pore formation mechanism

In order to further study the porous features in Fig. 4c, SEM characterization at a higher magnification was performed, as shown in Fig. 6a. It was clear that the dense metallic agglomerates joined together via sintering necks (arrowheads, Fig. 6a), leaving inter-agglomerate residual porosity. Fig. 6b schematically depicts the formation mechanisms of pores during DMLS. When the laser beam scans over the loose powder bed at a constant speed, several powder particles are irradiated simultaneously in each laser-irradiating zone, due to a larger laser spot size (300 μm) relative to powder
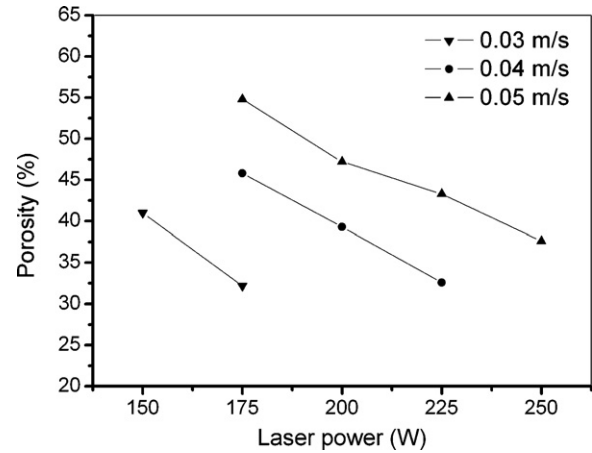

Fig. 7. Variation of porosity of laser sintered porous samples with laser power and scan speed. Fixed parameters are h = 0.15 mm and d = 0.15 mm.

particle size (20 μm) in this study (Stage I). The laser energy is primarily absorbed in a narrow layer of individual powder particles, leading to a high temperature of the surface of particles during the interaction. The heat, subsequently, flows mainly towards the centre
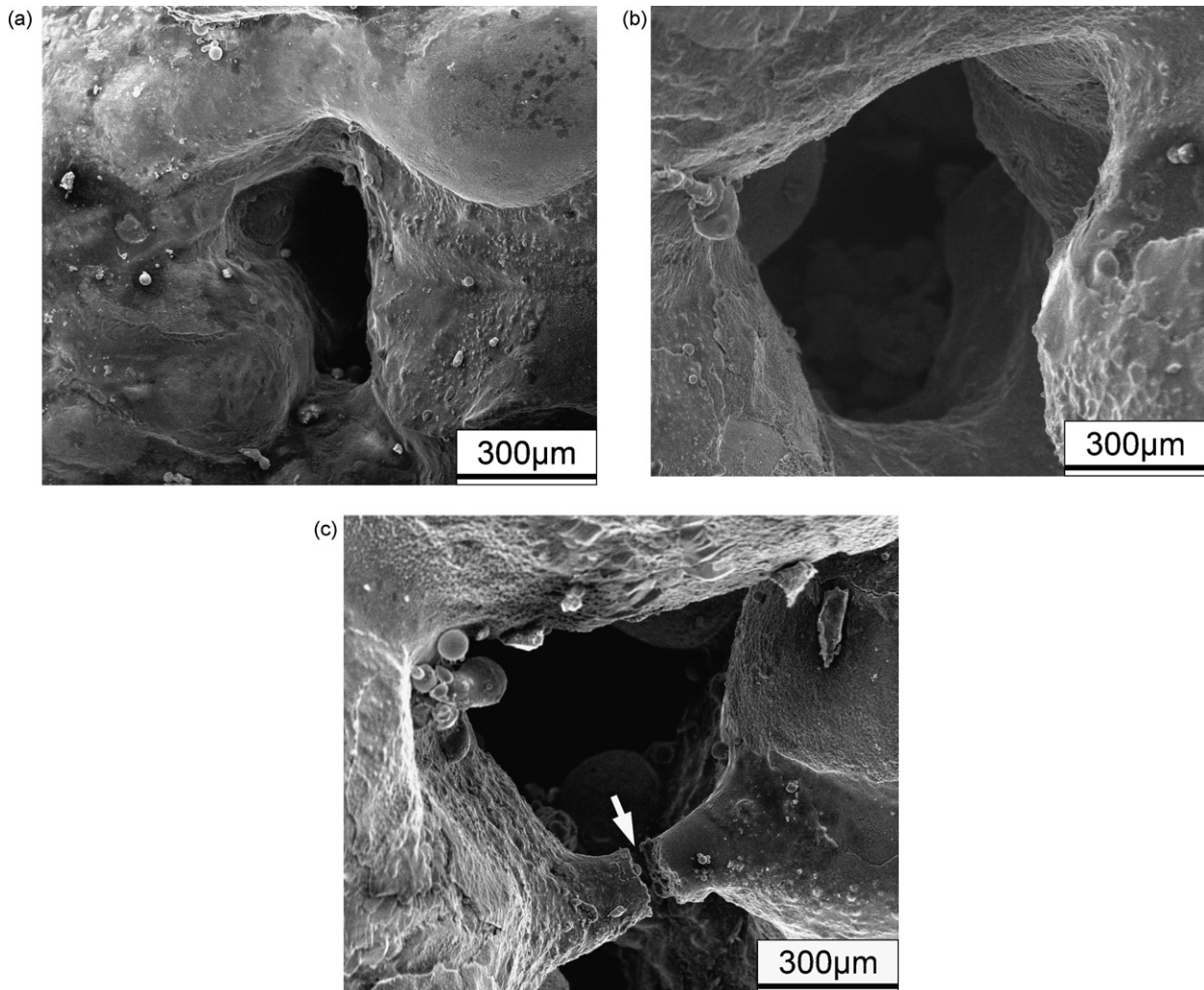

Fig. 8. SEM images showing characteristic pore features in laser sintered porous samples prepared at: (a) P = 225 W, v = 0.04 m/s; (b) P = 175 W, v = 0.04 m/s; (c) P = 175 W, v = 0.05 m/s. Fixed parameters are h = 0.15 mm and d = 0.15 mm.

of particles until a local steady state of the temperature within the particles is obtained [25]. With suitable processing conditions determined (Figs. 3 and 5), the surface of particles melts to form liquid, while the cores of particles remain in solid. The liquid quickly collects at particle interfaces, forming liquid "bridges" between solid particles (Stage II). With the laser beam moving away, the surface-melted particles join together due to the presence and combination of sintering necks, leaving residual pores between solidified metallic agglomerates (Stage III).

3.3. Influence of processing parameters on porosity and microstructure

With the above mentioned process map defined, the porous structures are generally obtainable in laser sintered SS components through the partial melting mechanism. However, the microstructural characteristics of pores show some distinct changes with various processing conditions. The influence of processing parameters (e.g., laser power, scan speed, scan line spacing, and power layer thickness) is highlighted as follows.

3.3.1. Influence of laser power and scan speed

Although laser sintering using the parameters within Zone II (Fig. 3) generally led to a favorable mechanism of powder melting and the resultant desirable porous structure, the amount of porosity and the microstructural features of pores varied considerably with the processing conditions. Fig. 7 depicts the influence of processing parameters on the sintered porosity. It was found that ∼32–∼55% porosity was generally obtainable after sintering. However, for a given scan speed, the porosity decreased with increasing the laser power. When the laser power was fixed, a higher porosity was obtainable for a higher scan speed. The characteristic morphologies of pores on surfaces of laser sintered samples are provided in Fig. 8. The features of porous structures, e.g., pore size, metal agglomeration size and shape, neck size and connectivity, showed a distinct variation with the used parameters. At a relatively high laser power of 225 W and a relatively low scan speed of 0.04 m/s, the sintered metallic agglomerates were large-sized and the sintering necks were well developed, forming small-sized residual pores (Fig. 8a). With lowering the laser power to 175 W, laser sintering at the same scan speed led to the formation of round and large pores with the diameter of ∼750 μm (Fig. 8b). Keeping the laser power fixed, increasing the scan speed to 0.05 m/s led to a further increase in the sintered porosity (Fig. 7). However, a fraction of necks between the sintered agglomerates became thinner and interrupted (arrowhead, Fig. 8c).
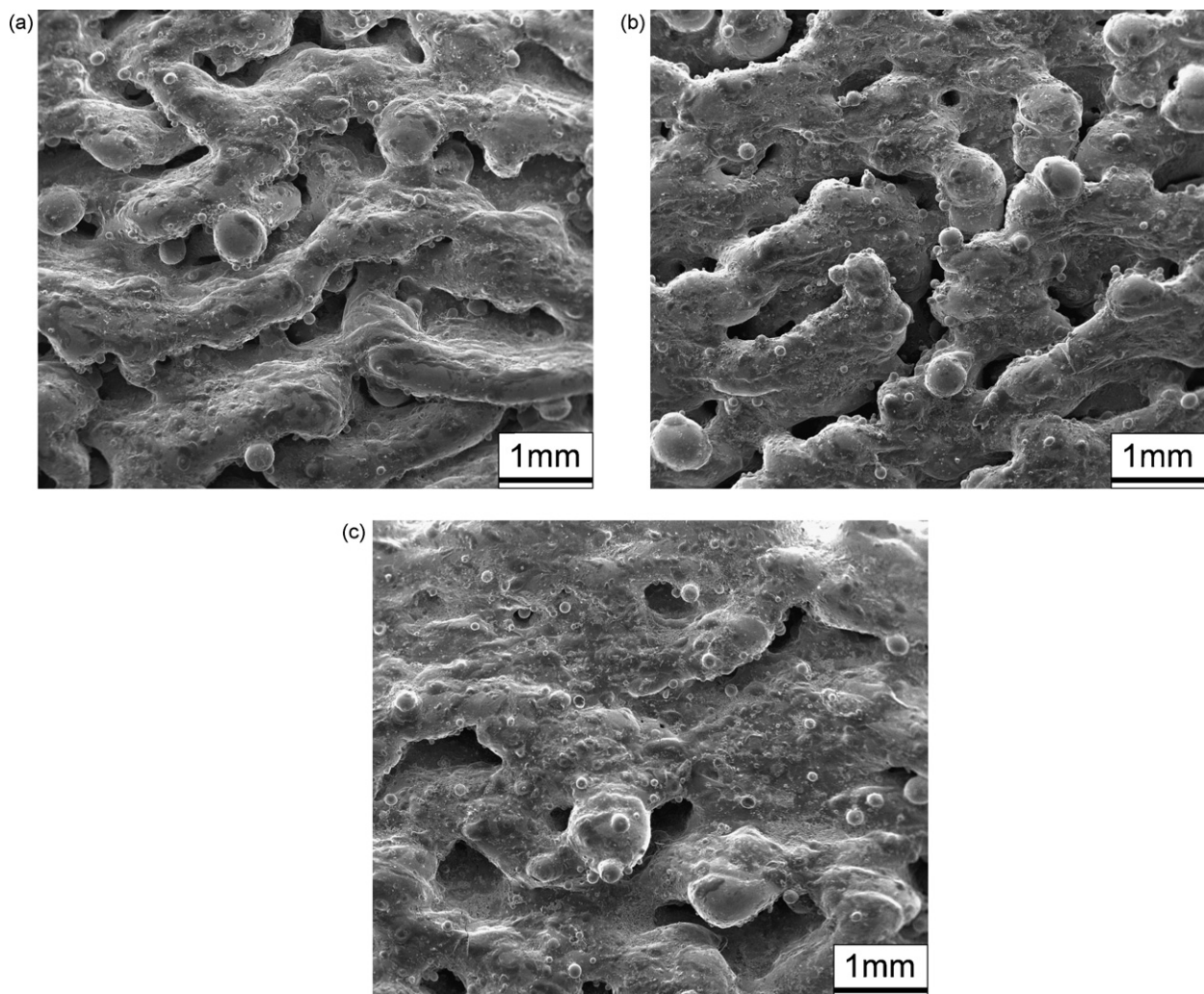

Fig. 9. SEM images showing typical surface morphologies of laser sintered porous samples with various scan line spacing: (a) $h = 0.30$ mm, (b) $h = 0.15$ mm, and (c) $h = 0.10$ mm. Fixed parameters are $P = 225$ W, $v = 0.04$ m/s, and $d = 0.15$ mm.

In general, a partial melting of powders occurs within Zone II of Fig. 3 as the obtained sintering temperature falls between the solidus and liquidus temperatures of SS powder, which favors the formation of porous structures (Fig. 6). On the other hand, SS powder, which melts incongruently within such a temperature range, exhibits a higher degree of liquid formation as the temperature above the solidus increases. As the laser power increases or the scan speed decreases, the amount of energy absorbed by the powders under the laser beam enhances, inducing a larger degree of melting. Consequently, the size of the solidified metallic agglomerates and the inter-agglomerate sintering necks increases, thereby decreasing the size of the residual pores (Fig. 8a) and thus the obtainable sintered porosity (Fig. 7). In other words, as the favorable partial melting mechanism prevails, a reasonable decrease in laser powder (Fig. 8b) or a moderate increase in scan speed (Fig. 8c) generally leads to a higher porosity in laser sintered powders. However, it is noted that although a higher porosity is obtainable with the combination of a low laser power and a high scan speed, some sintering necks become thinner and interrupted (Fig. 8c), which ultimately lower the continuity of the porous structure. Therefore, care should be taken to choose the optimal processing parameters within the suitable process window (Zone II, Fig. 3) in order to yield a sufficiently high porosity combined with an adequate structural continuity.

3.3.2. Influence of scan line spacing

The characteristic surface morphologies of laser sintered porous samples at different scan line spacing are provided in Fig. 9. It raveled that the microstructural features (e.g., the size and shape of sintered agglomerates, the shape and connectivity of pores, and the amount of porosity) were significantly influenced by the used scan line spacing. At a large line spacing of 0.30 mm, long and narrow sintered agglomerates were formed, between which interconnected pore channels in the order of millimeter were visible (Fig. 9a), thereby leaving a high residual porosity, i.e., 41.3%, in laser sintered component. Laser sintering at a lower line spacing of 0.15 mm produced the relatively large sintered agglomerates and the discontinuously distributed inter-agglomerate pores (Fig. 9b), resulting in a decrease in the obtainable porosity (33.6%). As the line spacing further decreased to 0.10 mm, a denser sintered surface consisting of a small amount of pores was present (Fig. 9c), leading to a sharp decrease in porosity (20.7%). Thus, it is reasonable to conclude that a suitable increase in scan line spacing leads to a higher sintered porosity.

As mentioned above, laser sintering of SS powder involves the melting of particle surfaces but the remaining of particle cores. It is known that when localized powder melting occurs during laser scanning, a significant temperature gradient tends to form between the centre and edge of the molten pool, due to a Gaussian laser beam used. Both concentration differences and temperature gradients at solid–liquid interfaces can give rise to surface tension gradients and resultant Marangoni flows [16–18,24]. The convective Marangoni streams tend to rotate the SS particle cores within the pool and, meanwhile, moves them towards the centre of laser beam, where the temperature is maximum [26]. Thus, arrays of agglomerates at the centre of the scanned tracks and the interconnected inter-track pores were formed (Fig. 9a). Narrowing the scan line spacing makes the adjacent scan tracks close to each other until they overlap. Thus, a portion of laser spot tends to scan over the previously sintered track, favoring the remelting of the primarily processed materials and, accordingly, the escaping of the previously trapped air. The liquid, therefore, can flow and spread easily between the adjacent tracks, thereby decreasing the porosity in finally solidified materials (Fig. 9b and c).

3.3.3. Influence of powder layer thickness

Fig. 10 depicts the variation of laser sintered porosity with the used powder layer thickness. It was clear that when other processing parameters were constant, the obtainable sintered porosity decreased with lowering the powder layer thickness. The decreasing tendency became more significant for a smaller layer thickness.

It is known that a large amount of air exists in the pores between particles in a loose powder layer, and tends to be trapped as bubbles when the powder layer undergoes laser-induced melting [27]. For a fixed laser energy input, the thinner the powder layer is, the deeper the laser beam penetrates into the layer, leading to a larger degree of melting. Thus, most of air bubbles, even at the bottom of the layer, are able to move up to the surface of the layer, and collapse when the liquid solidifies rapidly, leading to less sintered porosity.

3.4. Stress–strain response

Typical stress–strain curves of laser sintered porous sample are provided in Fig. 11. Fig. 11a presents the tensile test performed parallel to the sintered layers. The curve showed a nearly linear elastic behavior at small strains, followed by yield and strain hardening up to a peak stress. The ultimate tensile strength of the sample was 152 MPa. It is known that the weakest direction of parts produced by DMLS is the building direction (i.e., perpendicular to the
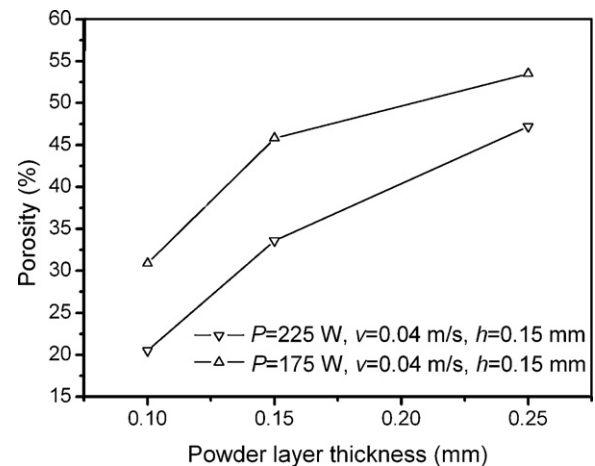

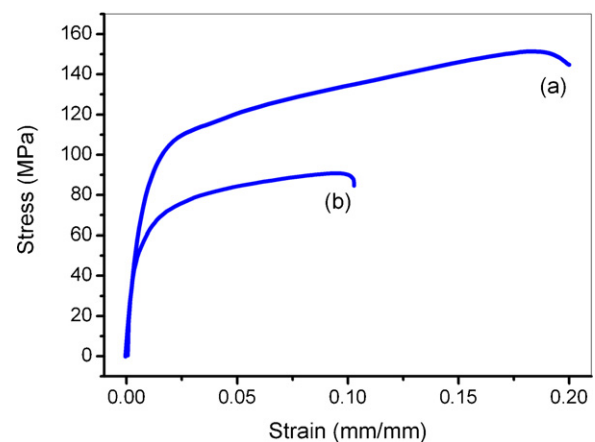**Fig. 10.** Effect of powder layer thickness on porosity of laser sintered porous samples.

Fig. 11. Stress–strain curves for laser sintered porous SS sample prepared at $P = 250$ W, $v = 0.05$ m/s, $h = 0.15$ mm, and $d = 0.15$ mm. The tensile tests are performed parallel to (a) and perpendicular to (b) the sintered layers, respectively.

sintered layers). The tensile test performed in this direction revealed that the ultimate tensile strength showed a certain degree of decrease, i.e., 91 MPa (Fig. 11b). After a combined evaluation, it is reasonable to consider that DMLS process holds a high potential for obtaining porous SS components possessing a sufficient strength.

4. Conclusions

Based on the experiments conducted, the following conclusions can be drawn:

(1) Tailoring a partial melting mechanism showed a high feasibility in obtaining a porous laser sintered structure. The combination of a moderate linear energy density of ∼3400–∼6000 J/m and a lower scan speed less than 0.06 m/s contributed to the presence of a feasible sintering mechanism.
(2) With a suitable sintering mechanism determined, a reasonable decrease in laser power or an increase in scan speed, scan line spacing, and powder layer thickness generally led to a higher sintered porosity.
(3) Porosities of ∼21–∼55% were generally obtainable in laser sintered samples. A favorable stress–strain response, i.e., the tensile strength of 152 MPa, was obtained under optimal processing conditions.
(4) The presence of pores in laser sintered porous metals was through: (i) the formation of liquid bridges between partially melted particles during laser irradiation; and (ii) the presence and growth of sintering necks during solidification, leaving residual pores between solidified metallic agglomerates.

Acknowledgements

References

[1] M.F. Ashby, A. Evans, N.A. Fleck, L.J. Gibson, J.W. Hutchinson, H.N.G. Wadley, Metal Foams: A Design Guide, 1st ed., Butterworth-Heinemann, Oxford, 2000.
[2] L.J. Gibson, M.F. Ashby, Cellular Solids: Structure and Properties, 2nd ed., Cambridge University Press, Cambridge, 1997.
[3] J. Banhart, Prog. Mater. Sci. 46 (2001) 559.
[4] W.H. Lee, C.Y. Hyun, Appl. Surf. Sci. 252 (2006) 4250.
[5] W.H. Lee, C.Y. Hyun, J. Mater. Process. Technol. 189 (2007) 219.
[6] S. Esmaeelzadeh, A. Simchi, D. Lehmhus, Mater. Sci. Eng. A 424 (2006) 290.
[7] B. Matijasevic-Lux, J. Banhart, S. Fiechter, O. Görke, N. Wanderka, Acta Mater. 54 (2006) 1887.
[8] Z.S. Rak, J. Walter, J. Mater. Process. Technol. 175 (2006) 358.
[9] Y. Yamada, K. Shimojima, Y. Sakaguchi, M. Mabuchi, M. Nakamura, T. Asahina, T. Mukai, H. Kanahashi, K. Higashi, Adv. Eng. Mater. 2 (2000) 184.
[10] W. Xue, B.V. Krishna, A. Bandyopadhyay, S. Bose, Acta Biomater. 3 (2007) 1007.
[11] B.V. Krishna, S. Bose, A. Bandyopadhyay, Acta Biomater. 3 (2007) 997.
[12] J.M. Williams, A. Adewunmi, R.M. Schek, C.L. Flanagan, P.H. Krebsbach, S.E. Feinberg, S.J. Hollister, S. Das, Biomaterials 26 (2005) 4817.
[13] D.A. Hollander, M. von Walter, T. Wirtz, R. Sellei, B. Schmidt-Rohlfing, O. Paar, H.J. Erli, Biomaterials 27 (2006) 955.
[14] I. Shishkovsky, Yu. Morozov, I. Smurov, Appl. Surf. Sci. 254 (2007) 1145.
[15] I. Yadroitsev, Ph. Bertrand, I. Smurov, Appl. Surf. Sci. 253 (2007) 8064.
[16] D.D. Gu, Y.F. Shen, Appl. Surf. Sci. 254 (2008) 3971.
[17] D.D. Gu, Y.F. Shen, Mater. Sci. Eng. A 435–436 (2006) 54.
[18] D.D. Gu, Y.F. Shen, L. Zhao, J. Xiao, P. Wu, Y.B. Zhu, Mater. Sci. Eng. A 445–446 (2007) 316.
[19] A.J. Pinkerton, L. Li, Appl. Surf. Sci. 208–209 (2003) 411.
[20] A.J. Pinkerton, L. Li, Appl. Surf. Sci. 208–209 (2003) 405.
[21] J.D. Majumdar, A. Pinkerton, Z. Liu, I. Manna, L. Li, Appl. Surf. Sci. 247 (2005) 320.
[22] J.D. Majumdar, A. Pinkerton, Z. Liu, I. Manna, L. Li, Appl. Surf. Sci. 247 (2005) 373.
[23] D.D. Gu, Y.F. Shen, J. Mater. Process. Technol. 182 (2007) 564.
[24] A. Simchi, H. Pohl, Mater. Sci. Eng. A 359 (2003) 119.
[25] P. Fischer, V. Romano, H.P. Weber, N.P. Karapatis, E. Boillat, R. Glardon, Acta Mater. 51 (2003) 1651.
[26] H.J. Niu, I.T.H. Chang, Scripta Mater. 41 (1999) 25.
[27] A.N. Chatterjee, S. Kumar, P. Saha, P.K. Mishra, A.R. Choudhury, J. Mater. Process. Technol. 136 (2003) 151.